



Nonadiabatic dynamics and photoisomerization of biomimetic photoswitches

Deping Hu ^{a,b}, Jing Huang ^{a,b}, Yu Xie ^a, Ling Yue ^{c,d}, Xuhui Zhuang ^{a,b}, Zhenggang Lan ^{a,b,*}

^a Key Laboratory of Biobased Materials, Qingdao Institute of Bioenergy and Bioprocess Technology, Chinese Academy of Sciences, Qingdao 266101, Shandong, People's Republic of China

^b University of Chinese Academy of Sciences, Beijing 100049, People's Republic of China

^c School of Science, Department of Chemistry, Xi'an Jiaotong University, Xi'an 710049, People's Republic of China

^d Key Laboratory of Theoretical and Computational Photochemistry, Ministry of Education, College of Chemistry, Beijing Normal University, Beijing 100875, People's Republic of China



ARTICLE INFO

Article history:

Received 17 July 2015

In final form 11 October 2015

Available online 23 October 2015

Keywords:

NAIP

Nonadiabatic dynamics

Photoswitch

Photoisomerization

Surface hopping

Semi-empirical method

ABSTRACT

N-alkylated indanylidene pyrrolidine Schiff bases (NAIPs) are of great interest because their photoisomerization mimics the primary photoreactions of the retinal chromophore in rhodopsin. The nonadiabatic dynamics of two NAIP models (OMe-NAIP and dMe-OMe-NAIP) are investigated by trajectory surface-hopping method at the semi-empirical OM2/MRCI level. Both molecules show ultrafast isomerization governed by nonadiabatic dynamics via the S_0/S_1 conical intersections (CIs). Two CIs, Cl_α and Cl_β , play important roles in the $E \rightarrow Z$ and $Z \rightarrow E$ isomerization dynamics, respectively, and are mainly distinguished by different twisting statuses of the central $C1'-C4$ double bond. Although both compounds show ultrafast nonadiabatic dynamics, the S_1 lifetime of dMe-OMe-NAIP is much longer than that of OMe-NAIP. By removing the methyl group, dMe-OMe-NAIP allows less twist at the $C1'-C4$ double bond than OMe-NAIP. This result in the slower excited-state decay of dMe-OMe-NAIP, providing solid evidence to support a similar hypothesis proposed in a previous study.

© 2015 Elsevier B.V. All rights reserved.

1. Introduction

Molecular switches have been intensively studied for several years [1,2] because their physical, chemical and biological properties can be controlled by external stimulation, e.g., pH, light, temperature, electric fields. Photoinduced molecular switches are compounds that experience geometry transformation upon light excitation; these play important roles in sensors [3,4], self-assembly [5,6] and photoinduced biological processes [7–9]. Recently, photoswitches based on the E/Z isomerization have become of great interest. These compounds normally contain C-C, C-N and N-N double bonds and the resulting two configurations (E and Z) can be converted to each other after photoabsorption [10–15]. Several families of E/Z photoswitches have been constructed in recent years, including azobenzenes [16–21], chiral diarylidenes [22–25] and protonated Schiff bases (PSB, mimicking the retinal chromophore of rhodopsins) [26–30]. Due

to their photo-controlled properties, these photoswitches have potential applications in several fields [31–34].

One particularly interesting group of photoswitches is based on N-alkylated indanylidene pyrrolidine Schiff bases (NAIPs) and their derivatives. They serve as simplified biomimetic models to investigate the photoisomerization mechanism of retinal chromophores in rhodopsin [35–41]. In addition, the functionalization of NAIP-based compounds helps us to develop novel biomimetic photoswitches for future applications [42–46]. Consequently, a good understanding of the photoinduced E/Z isomerization of NAIP-based compounds is critical.

Both time-resolved spectroscopies and quantum-chemical calculations suggest that the photoinduced E/Z isomerization of NAIP-based switches is governed by an ultrafast nonadiabatic process via the S_0/S_1 conical intersections (CIs) [42–46]. After photoexcitation, the NAIP-family molecules move in the excited state, access the S_0/S_1 CIs by twisting the central C-C double bond, then jump back to the ground state [42–46]. A joint experimental-theoretical study was performed to understand the E/Z isomerization of OMe-NAIP (Scheme 1), a NAIP derivative with an $-OCH_3$ group attached to the six-membered ring [44]. The experimental observations suggested that the excited-state lifetime is approximately 300 fs, which is consistent with the value (~ 200 fs) obtained by the theoretical simulation using trajectory calculations on the basis

* Corresponding author at: Key Laboratory of Biobased Materials, Qingdao Institute of Bioenergy and Bioprocess Technology, Chinese Academy of Sciences, Qingdao 266101, Shandong, People's Republic of China. Tel.: +86 532 80662630; fax: +86 532 80662778.

E-mail address: lanzg@qibebt.ac.cn (Z. Lan).

of the reduced dimensional potential-energy model constructed in the combined CASSCF/CASPT2/AMBER approach [44]. Subsequently, the excited-state dynamics of another NAIP derivative was explored by theoretical simulation using a few typical trajectories at the scaled CASSCF/AMBER level [43] which suggested that the nonadiabatic decay takes place ~ 300 fs. These theoretical studies employed very accurate high-level electronic-structure methods and even considered the QM/MM approach to account for solvent effects, all of which requires huge computational costs.

Recently, a new biomimetic photoswitch, dMe-OMe-NAIP (**Scheme 1**), was constructed by removing the methyl group from the pyrrolinium in the structure of OMe-NAIP [47]. Time-resolved spectroscopy studies indicate that the lifetime of dMe-OMe-NAIP is above 500 fs, much longer than that of OMe-NAIP. This strongly suggests that the removal of the methyl group has a dramatic influence on the E/Z isomerization of NAIP derivatives. Simple ground-state geometry calculations indicate a possible explanation of this effect: the removal of the methyl group reduces the central double-bond twisting angle and the resulting more planar geometry may be responsible for the slower isomerization dynamics of dMe-OMe-NAIP [47].

From a theoretical point of view, it is essential to simulate the reaction dynamics to provide direct evidence of the influence of removing the methyl group on the E/Z isomerization. One possibility of examining such phenomena is to run nonadiabatic dynamics simulations of both NAIP derivatives (dMe-OMe-NAIP and OMe-NAIP) with on-the-fly surface-hopping methods. By employing a large number of trajectories and including all nuclear degrees of freedom (full dimensionality), more details on the nonadiabatic dynamics of dMe-OMe-NAIP and OMe-NAIP are derived. When the high-level electronic structure methods (such as CASSCF) were employed, the dynamics study is only possible for the small simplified model systems [42]. Here, we wish to simulate the E/Z isomerization dynamics of realistic systems, dMe-OMe-NAIP and OMe-NAIP, with on-the-fly surface-hopping and the Tully-fewest switches algorithm [48–50]. Because we need enough trajectories to achieve a statistically meaningful conclusion, the semi-empirical OM2/MRCI method was employed to speed up the calculations. As discussed in many previous studies, the OM2/MRCI method provides a reasonable compromise between computational cost and accuracy in the nonadiabatic dynamics simulations of many photochemical processes [21,51–63], particular for

middle-sized molecular systems. Certainly, the performance of the OM2/MRCI method should be examined by the benchmark calculations with high-level ab initio method for validation purpose.

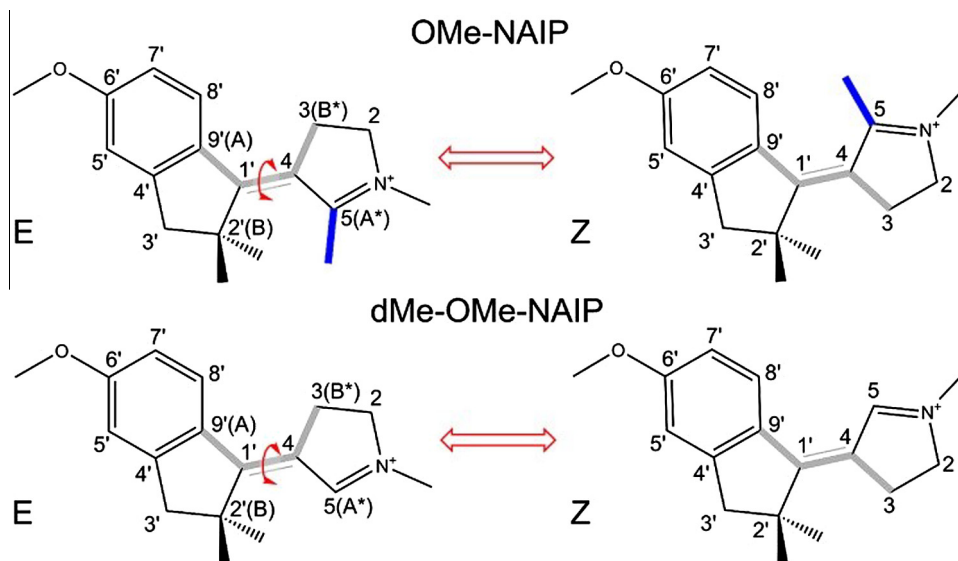
This article is organized as follows: first, the computational details are described, including the molecular models, the OM2/MRCI method and the surface-hopping method. To test the accuracy of the OM2/MRCI method, high-level calculations were also applied for validation. Second, the results for OMe-NAIP and dMe-OMe-NAIP, including PESs and nonadiabatic dynamics, are presented. Third, the discussion section is given. Finally, we summarize the whole work.

2. Computational details

2.1. Molecular models

The current work focuses on the photoinduced E \rightarrow Z and Z \rightarrow E isomerization processes of two NAIP switches, namely OMe-NAIP and dMe-OMe-NAIP (**Scheme 1**). Both have two isomers: E-OMe-NAIP and Z-OMe-NAIP for OMe-NAIP and E-dMe-OMe-NAIP and Z-dMe-OMe-NAIP for dMe-OMe-NAIP. Their chemical structures and atomic labeling are shown in **Scheme 1** and all key geometry parameters are listed in **Table 1**. In this table, the central double bond (C1'-C4) length is defined by r_a . The dihedral angle C9'-C1'-C4-C3 (τ_a) describes the twisting motion around the C1'-C4 double bond. The dihedral angles C9'-C2'-C4-C1' (τ_b) and C3-C1'-C5-C4 (τ_c) describe the pyramidalizations at the C1' and C4 atoms, respectively. The five-membered ring distortion is described by the dihedral angle C4-C3-C2-C5 (τ_d). The five-membered ring moiety and the double-ring panel are defined as the “rotator” and “base”, respectively. For convenience, the switch process always refers to the twisting motion of the rotator with respect to the base.

In our two simulated molecules, OMe-NAIP and dMe-OMe-NAIP, the rotator is connected to the base by the C1'-C4 double bond (**Scheme 1**). Because the rotation of the five-membered ring with respect to the base may be clockwise or counter-clockwise, two different configurations exist for the same E (or Z) isomers (**Scheme 2**). In fact, these two configurations with different orientations are explained by the P/M chirality [64]. According to the different substituents along the rotation axis (C1'-C4 double bond) (**Scheme 1**), the P and M chirality can be defined as follows: first,



Scheme 1. The E \rightarrow Z and Z \rightarrow E isomerization of OMe-NAIP (top) with the methyl group and dMe-OMe-NAIP (bottom) without the methyl group.

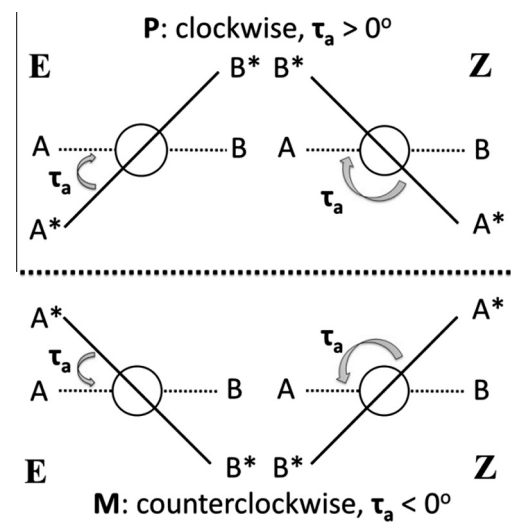
the priority of all four substituents are assigned based on Cahn–Ingold–Prelog rules [65]. We defined the A and B atoms to be located on the base, whereas A^* and B^* are located on the rotator. In principle, $C9'$ has higher priority than $C2'$ because $C9'$ is connected to $C8'$ (belonging to the aromatic ring) and $C2'$ is connected to the $-CH_3$ group. Thus A and B correspond to $C9'$ and $C2'$, respectively. For similar reasons, we assign A^* and B^* to $C5$ and $C3$, respectively. Second, the A–B part (base) is always put behind the A^*-B^* part (rotator, Scheme 2). Following the shortest rotation pathway from the A^* atom in the A^*-B^* rotator to the A atom in the A–B base, clockwise motion defines the P configuration and counter-clockwise motion gives the M configuration (Scheme 2). Here, the rotation of the five-membered ring is described by $C9'-C1'-C4-C3$ (τ_a), and thus a positive value defines the clockwise rotation (P chirality) and a negative value defines the counter-clockwise rotation (M chirality). Note that the P/M chirality is unchanged when we reverse the labeling of the rotator and the base. Several previous studies have tried to define the chirality of similar systems of molecular rotors while using quite different explanations of the chirality [43,44,66], such as deriving the helicity based on the insertion of a stereogenic center in particular atomic positions ($C3$, $C2$ in NAIPs). Our main task, however, is to describe the helicity distinguished by different orientations of the internal rotation along the $C1'-C4$ axis. Thus, the P and M helicity is defined by the counter-clockwise and clockwise rotation of the rotator with respect to the base. Also for this purpose, the Cahn–Ingold–Prelog rule was taken to assign the priority of all four substituent atoms (A, B and A^* , B^*). Consequently, no contradiction exists in the P/M chirality assignments between the current work and previous ones, although great caution should be taken to avoiding misunderstandings from incorrect comparisons.

2.2. Electronic-structure calculations

2.2.1. Semi-empirical OM2/MRCI method

All semi-empirical calculations were performed with the development version of the MNDO99 program [67]. The semi-empirical OM2/MRCI method (orthogonalization model 2 and multireference configuration interaction) [51–53] was used to describe excited-state wave functions. The Self-Consistent Field (SCF) calculations were performed with the restricted open-shell Hartree–Fock (ROHF) formalism, as previous work pointed out that it avoids some convergence problems associated with restricted Hartree–Fock (RHF) at the geometries close to the conical intersections [68,69]. This means that the molecular orbitals are generated from the open-shell singlet calculations. Three references (the closed-shell, single and double HOMO–LUMO excitations) were used to build all configurations in the MRCI expansion. The active space (AS) includes 14 electrons in 14 orbitals [AS (14, 14)] is chosen, since it provides the results consistent with those obtained at high levels [CASSCF/CASPT2 and SCS-ADC(2)]. All the single/double excitations within the AS were included in the configuration-interaction treatment.

Geometry optimizations of the ground-state and the excited-state minima were performed using the Newton–Raphson iteration scheme. The minimum-energy structures of the CIs were obtained



Scheme 2. Definition of P and M chirality for NAIPs: A–B [$A (C9')$, $B (C2')$] refers to the two-ring panel (base), A^*-B^* [$A^* (C5)$, $B^* (C3)$] refers to the five-membered ring moiety (rotator).

with the Lagrange–Newton method [69,70]. The reaction pathways were constructed by linear interpolations between the relevant minima and CIs. The CI seam was obtained by starting from the CI minimum energy geometry, then changing the structure by distortion along τ_a . The CI seam was then obtained by constrained CI optimization with fixed τ_a .

2.2.2. High-level ab initio calculations

For comparison, single-point calculations at critical points were performed at higher levels of theory: CASSCF/CASPT2 [71]/6-31G* and SCS-ADC(2) [72–75]/TZVP using MOLCAS 7 [76,77] and TURBOMOLE [78], respectively. At the CASSCF/CASPT2/6-31G* level, the complete active space (CAS) includes 12 electrons in 11 orbitals [CAS (12, 11)]: six π orbitals and five π^* orbitals.

2.3. Nonadiabatic dynamics

Photoinduced nonadiabatic dynamics were studied by trajectory surface-hopping simulation with Tully's fewest-switches algorithm [50]. A series of initial points in phase space (geometries and velocities) were generated stochastically based on the Wigner distribution function of the vibrational normal mode in the ground state [79]. The initial conditions were then created by putting these snapshots vertically into the S_1 state. One of the main purposes in this work is to understand the different nonadiabatic dynamics feature of two systems. The experimental studies on dMe-OME-NAIP mainly employed the laser excitation at 400 nm [47]. The excitation laser with similar wavelength (388–420 nm) was also used in the study of OMe-NAIP [44]. In both cases, only the S_1 state is excited. Thus all trajectories dynamics calculations start from the S_1 state.

All relevant energies, gradients and nonadiabatic couplings were calculated analytically along the trajectory propagation on-the-fly. The step time was 0.1 fs for the nuclear motion and 0.001 fs for the electronic propagation. The approach proposed by Persico and Granucci was taken to account the decoherence effect and the correction parameter is set as $C = 0.1$ Hartree [80]. The final results were obtained by averaging over a large number of trajectories: 149 for E-OMe-NAIP, 136 for Z-OMe-NAIP, 145 for E-dMe-OMe-NAIP and 126 for Z-dMe-OMe-NAIP.

Table 1
Important Internal coordinates.

Label	Internal coordinate	Motion
r_a	Distance $C1'-C4$	$C1'-C4$ stretching
τ_a	Dihedral angle $C9'-C1'-C4-C3$	Twisting around $C1'-C4$
τ_b	Dihedral angle $C9'-C2'-C4-C1'$	Pyramidalizations at $C1'$
τ_c	Dihedral angle $C3-C1'-C5-C4$	Pyramidalizations at $C4$
τ_d	Dihedral angle $C4-C3-C2-C5$	Five-membered ring distortion

3. Results

For OMe-NAIP and dMe-OMe-NAIP, both E and Z configurations coexist under natural conditions and experience photoisomerization. Thus both configurations were taken into account in the excited-state dynamics simulation. We first discuss the excited-state dynamics of OMe-NAIP. Because this system was studied by previous theoretical work, it is also useful to examine the reliability of our approach. Next, we discuss the nonadiabatic dynamics of dMe-OMe-NAIP. Finally, the similarity and differences in the dynamics of the two molecules are addressed to clarify the role of the methyl group. For the sake of simplicity, we discuss only the main issues here, whereas additional data are given in the [Supplementary Data \(SD\)](#).

3.1. OMe-NAIP

3.1.1. Potential energy surface

For E-OMe-NAIP, the S_0 minimum has two conformers (**P** and **M**), due to chirality, which are symmetrical to each other through a planar reflection ([Fig. 1](#); [Tables S1 and S2, in SD](#)). According to the definition of chirality, **P** and **M** can be distinguished by the sign of the twisting angles of the central C1'–C4 double bond (**P**: $\tau_a > 0^\circ$, **M**: $\tau_a < 0^\circ$, see SD). For similar reasons, the S_1 minimum and CIs (discussed below) also appear in pairs (two conformers). We choose one representative set of conformers (**M**) as the illustrative example below.

The $(ES_0)_{\min}^M$ is the M conformer of $(ES_0)_{\min}$, whose energy is set as the reference (0 eV). The distance (r_a) and twisting angle (τ_a) of the C1'–C4 double bond are 1.39 Å and -17° , respectively, which agrees well with the previous data [44]. At the $(ES_0)_{\min}^M$, the vertical energy of the lowest singlet excited state S_1 is 2.94 eV, also consistent with the experimental data and previous theoretical work [44]. For the M conformer, an excited-state minimum $(CI)_{\min}^M$ exists in the Frank-Condon (FC) region, which has geometry similar to $(ES_0)_{\min}^M$.

For Z-OMe-NAIP, the situation is very similar. We also find two co-existing isomers for the S_0 minimum [$(ZS_0)_{\min}^P$ and $(ZS_0)_{\min}^M$] and the S_1 minimum [$(ZS_1)_{\min}^P$ and $(ZS_1)_{\min}^M$] due to chirality ([Fig. 1](#); [Tables S1 and S2, in SD](#)). $(ZS_0)_{\min}$ is the global minimum, slightly lower (0.1 eV) than $(ES_0)_{\min}$. A similar vertical energy, 2.91 eV, of the S_1 state is found for the Z configuration. The twist of the C1'–C4 double bond ($\tau_a = -157^\circ$) is also observed at $(ZS_0)_{\min}^M$ (M conformer of $(ZS_0)_{\min}$), where the C1'–C4 double bond distance is 1.38 Å.

Four groups of S_1/S_0 conical-intersection minima are found at the OM2/MRCI level, which are differentiated by two key internal coordinates: the twisting angle around the C1'–C4 bond (τ_a) and the pyramidalization angle at the C1' atom (τ_b , [Fig. 1](#); [Tables S1 and S2, in SD](#)).

The first S_1/S_0 conical-intersection minimum $(CI)_{\alpha M}$ is located at 1.62 eV and is characterized by twisting around the C1'–C4 bond ($\tau_a = -75^\circ$), the strong pyramidalization of the C1' atom ($\tau_b = 16^\circ$), and the elongation of the C1'–C4 bond (1.44 Å). This strong pyramidalization may be caused by the sudden polarization effect [81] which is often observed in the photoisomerization of unsaturated molecules, such as ethylene [82] or xylene derivatives [61]. However, as a semi-empirical approach, the OM2/MRCI method may only give the qualitative description on the sudden polarization effect.

The second S_1/S_0 conical-intersection minimum $(CI)_{\beta}^M$ lies only slightly higher (0.05 eV) than the first one. The twisting around the C1'–C4 bond at $(CI)_{\beta}^M$ ($\tau_a = -103^\circ$) is different than the first one ($\tau_a = -75^\circ$), whereas the pyramidalization at the C1' atom

and the elongation of the C1'–C4 bond are similar to their counterparts at $(CI)_{\alpha}^M$

The third and fourth S_1/S_0 conical-intersection minimum $(CI)_{\gamma}^M$ and $(CI)_{\delta}^M$ are significantly different from $(CI)_{\alpha}^M$ and $(CI)_{\beta}^M$. Both are mainly characterized by the strongly deformation of the five-membered ring (the rotator), distinguished by the opposite direction of the C1'–C4 bond rotation. However, these two CIs do not play important roles in the isomerization dynamics (see below discussions on nonadiabatic dynamics).

The first two CIs were also mentioned by previous theoretical work [44], which are responsible for the main reaction channels (see below discussion). In addition, we also performed high-level electronic-structure calculations at the CASSCF/CASPT2 and SCS-ADC(2) levels based on the OM2/MRCI optimized geometries ([Tables S1 and S2, in SD](#)). At $(CI)_{\alpha}^M$ and $(CI)_{\beta}^M$ obtained at the OM2/MRCI, the S_0 – S_1 energy gaps are around 0.08–0.16 eV at the CASPT2 level. At the same geometries, a little larger energy gaps were observed at the CASSCF and ADC(2) level. Although the large differences were observed for $(CI)_{\gamma}^M$ and $(CI)_{\delta}^M$, these two conical intersections are not the main reaction channels. Concerning the generally reliable performance of CASPT2, the OM2/MRCI calculations give a reasonable description of all critical geometries in the E/Z isomerization of OMe-NAIP. In addition, the main reaction pathways at the OM2/MRCI level are basically consistent with these at the CASPT2 level (<0.2 eV deviation), see [Figs. S19 and S20 in SD](#).

3.1.2. Nonadiabatic dynamics of OMe-NAIP

The $E \rightarrow Z$ and $Z \rightarrow E$ dynamics were investigated by a surface-hopping simulation at the OM2/MRCI level. For E-OMe-NAIP, because two S_0 minima structures are symmetrical with each other, we chose one of them, $(ES_0)_{\min}^M$, as the reference geometry for initial sampling. A similar approach was employed for Z-OMe-NAIP, where we chose $(ZS_0)_{\min}^M$ is the starting point in initial sampling.

After photo-excitation to S_1 , both isomers, E-OMe-NAIP and Z-OMe-NAIP, display ultrafast $S_1 \rightarrow S_0$ decay ([Fig. 2\(a\)](#) and (b)). This dramatic decay appears between 100 fs and 400 fs, with more than 50% of the trajectories jumping to the S_0 state at approximately 250 fs. This agrees well with previous experimental work (approximately 200 fs). A similar timescale was also proposed by previous high-level calculations using a typical trajectory [43] or employing the reduced dimensional model [44]. Such high consistency provides strong evidence for a reasonable description of NAIP excited states by OM2/MRCI. In addition, our current simulation provides data with statistical reasonability by applying a large number of trajectories on full-dimensional surfaces. After approximately 1 ps, the population decay is essentially over and almost all trajectories jump back to the ground state.

To examine the influence of the higher states, the S_2 energies at all critical geometries are given in SD. It is clear that the S_2 state lies in a high energy domain. In addition, we also plot the S_2 – S_1 energy differences before the $S_1 \rightarrow S_0$ hops along the typical trajectory ([Figs. S23\(d\) and S24, in SD](#)) for OMe-NAIP and dMe-OMe-NAIP. The result shows that the S_2 – S_1 energy difference is always large along the trajectory. So the S_2 state is not relevant to the current simulation.

The Tully's surface hopping method makes an important assumption called "the internal consistency", which assumes that at any time the same values should be held for the average electronic population and fractional trajectory occupation [50]. This relation, however, could not be satisfied in many situations, particular for multi-dimensional systems [80,83–85]. Such problem can be alleviated by the so-called "decoherent corrections".

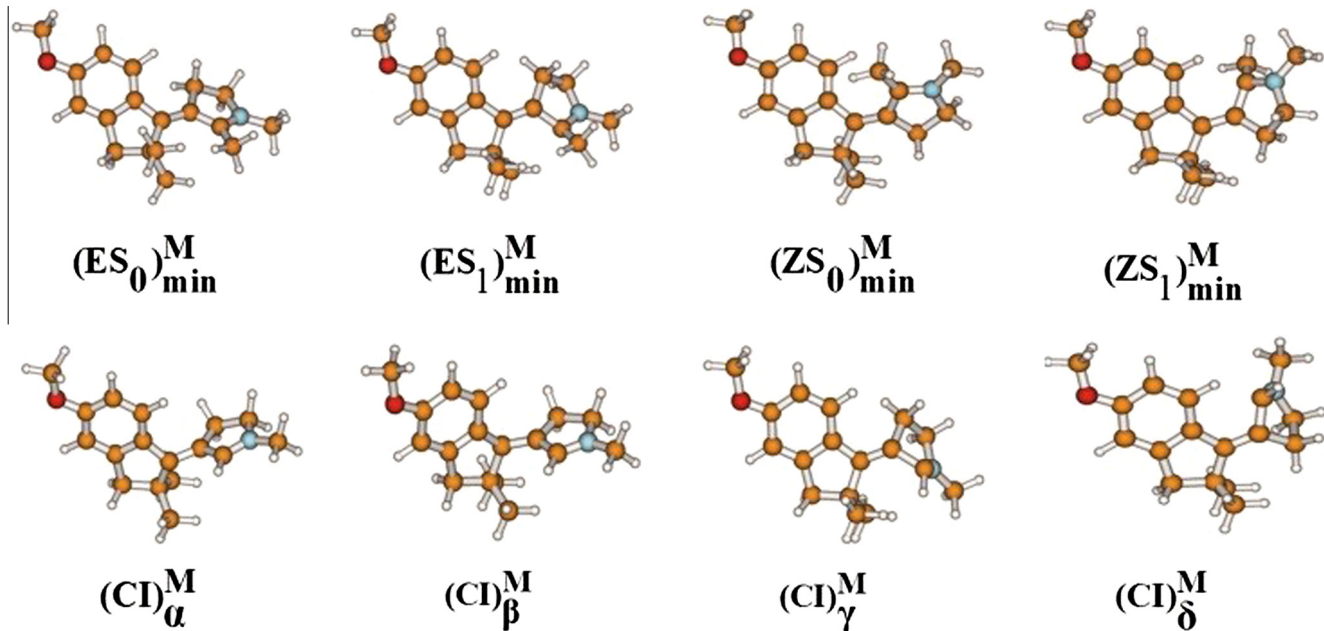


Fig. 1. The S_0 , S_1 minima and CIs with the **M** conformer of OMe-NAIP optimized at the OM2/MRCI level.

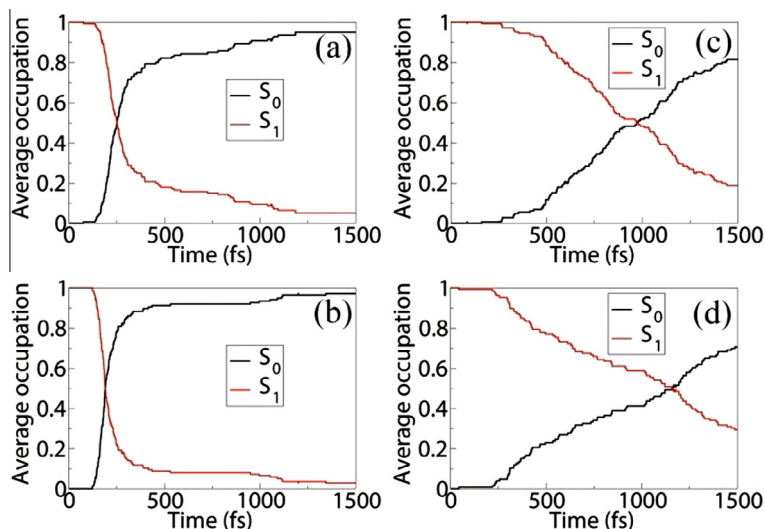


Fig. 2. Time-dependent average fractional occupations of electronic states for nonadiabatic dynamics initiated from: (a) $(ES_0)_\text{min}^M$ of E-OMe-NAIP; (b) $(ZS_0)_\text{min}^M$ of Z-OMe-NAIP; (c) $(ES_1)_\text{min}^M$ of E-dMe-OMe-NAIP; (d) $(ZS_1)_\text{min}^M$ of Z-dMe-OMe-NAIP.

We followed the approach by Granucci and Persico [80] to add the “decoherent corrections” in our nonadiabatic dynamics simulation. To examine the role of the “decoherent correction”, we also run the simulation for E-OMe-NAIP without “decoherent corrections” (Fig. 3(a) and (b)). The average electronic population and fractional trajectory occupation are not the same without decoherent corrections. However, these two quantities agree well after the “decoherent corrections” are introduced. Thus, the decoherent correction should be included to achieve the internal consistency in the surface-hopping dynamics.

To identify which CI conformation is responsible for the photoinduced nonadiabatic dynamics, geometrical distributions of the two key internal coordinates (τ_a and τ_b) at the initial time (Fig. 4(a) and (b)) and the $S_1 \rightarrow S_0$ hopping events (Fig. 4(c) and (d)) were built. Starting from $(ES_0)_\text{min}^M$ of E-OMe-NAIP, the

two-dimensional distribution at time zero is located at the FC region, with the center of the initial distribution located at $\tau_a = -17^\circ$. The majority of the trajectories pass the $(CI)_\alpha^M$ seam by a twisting motion around the C1'-C4 bond and the pyramidalization at C1'. Interestingly, the system undergoes a unidirectional rotation from $\tau_a \sim -17^\circ$ to $\tau_a \sim -75^\circ$ with the sign maintained during such motion. In other words, no trajectory enters the region of $\tau_a > 0^\circ$. Thus, a high selectivity of rotation direction was observed and the **M** chirality with respect to the C1'-C4 bond rotation remains unchanged. For Z-OMe-NAIP, most trajectories start from the FC point $[(ZS_0)_\text{min}^M]$ and pass the $(CI)_\beta^M$ seam, whereas only a minority decay via $(CI)_\alpha^M$. $(CI)_\alpha$ and $(CI)_\beta$ play important roles in the dynamics starting from the E and Z configurations, respectively.

In other words, the trajectories starting from the E/Z configurations may follow different pathways. Starting from the

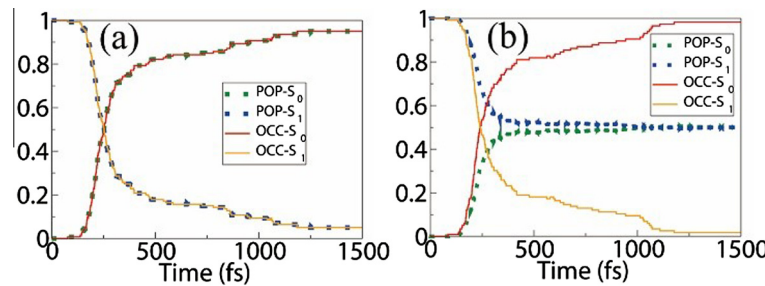


Fig. 3. Time-dependent average fractional occupations of electronic states for nonadiabatic dynamics initiated from $(ES_0)_{\min}^M$ of E-OMe-NAIP (a) with the decoherent correction and (b) without the decoherent correction, respectively.

E configuration, the C1'-C4 double bond must rotate further to reach $(Cl)_\beta$ and thus $(Cl)_\alpha$ is preferred. A few key conclusions can be drawn from further analysis of the dynamics: (a) an elongation of the C1'-C4 bond is observed when the system accesses the relevant Cls (Fig. S17, in SD), consistent with previous studies [43]; (b) trajectories access the Cl seams instead of the Cl minimum; (c) the sign of τ_a remains unchanged and thus the P/M chirality is maintained during the dynamical evolutions.

To illustrate the relation between the reaction products and the corresponding Cls, a branching ratio of the reaction channels was constructed and is shown in Fig. 5. From E-OMe-NAIP, most trajectories jump at $(Cl)_\alpha$ (Fig. 5(a)), consistent with the hop distribution (Fig. 4(b)).

After the $S_1 \rightarrow S_0$ hops at $(Cl)_\alpha$ similar numbers of trajectories move forwards to the Z configuration or backwards to the E configuration. For Z-OMe-NAIP, $(Cl)_\beta$ becomes dominant (Fig. 5(b)), whereas similar amounts of Z and E conformers are formed as the photoproducts. For both E-OMe-NAIP and Z-OMe-NAIP, side reactions via other two Cls [$(Cl)_\gamma$ and $(Cl)_\delta$] appear, though they play only minor roles here and are therefore neglected.

3.2. dMe-OMe-NAIP

3.2.1. Potential energy surface

Although the removal of the CH_3 group is the only difference between E-OMe-NAIP and E-dMe-OMe-NAIP, quite different ground-state geometries are obtained at the OM2/MRCI level.

First, only one S_0 and one S_1 minimum-energy structure were found for E-dMe-OMe-NAIP (Fig. 6; Tables S3 and S4, in SD). The $(ES_0)_{\min}$ of E-dMe-OMe-NAIP displays a planar structure with C_s symmetry. This is quite different from E-OMe-NAIP and eliminates the P/M isomer issue. At $(ES_0)_{\min}$, the vertical energy of the lowest singlet excited state S_1 was 3.0 eV, which is in good agreement with the available experimental absorption value 3.1 eV (400 nm) [47]. The planar S_1 minimum $(ES_1)_{\min}$ is also located near the FC region. Previous high-level calculations also predicted the geometry difference between E-OMe-NAIP and E-dMe-OMe-NAIP, although they identified a slight twisting angle of approximately 2° for E-dMe-OMe-NAIP. However, such a minor out-of-plane motion should not affect the dynamics, and our OM2/MCRI results are still reasonable. The geometry difference between E-OME-NAIP

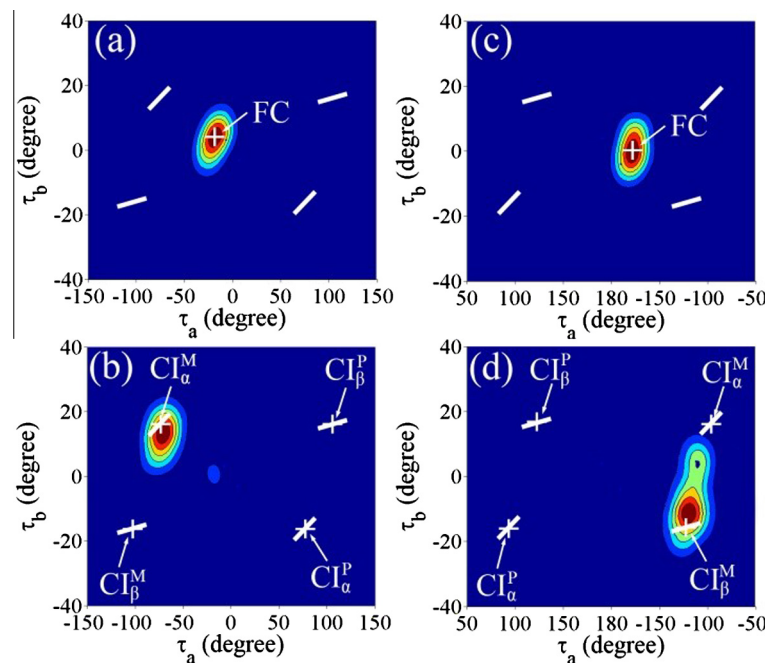


Fig. 4. Geometrical distributions of τ_a and τ_b at the: (a) initial steps for E-OMe-NAIP; (b) hopping steps for E-OMe-NAIP; (c) initial steps for Z-OMe-NAIP; (d) hopping steps for Z-OMe-NAIP. The white lines indicate the Cl seams. Note that the x axes (τ_a) in the above figures ([−150, 150] in the left column and [50, −50] in the right column) are not displayed in the same region.

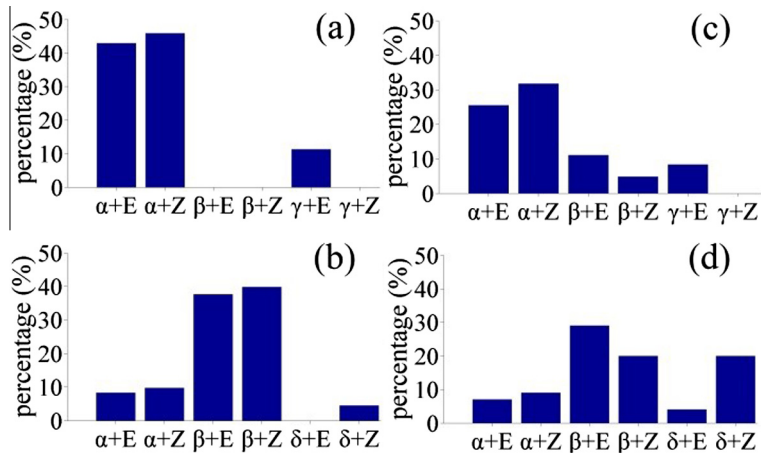


Fig. 5. Distributions of trajectories toward different reaction channels. “ $\theta + E/Z$ ” denotes the trajectories passing $(CI)_\theta$ ($\theta = \alpha, \beta, \gamma, \delta$) with E/Z products. Four different initial conditions are given: (a) E-OMe-NAIP; (b) Z-OMe-NAIP; (c) E-dMe-OMe-NAIP; (d) Z-dMe-OMe-NAIP.

and E-dMe-OMe-NAIP arises from the repulsive force between the methyl group at C5 and the two methyl groups attached to C2' in E-OMe-NAIP, causing a distortion along the C1'-C4 bond to avoid steric hindrance.

Z-dMe-OMe-NAIP and Z-OMe-NAIP show many similarities. Two S_0 minimum-energy structures [$(ZS_0)^P_{\min}$ and $(ZS_0)^M_{\min}$] and two S_1 minimum-energy structures [$(ZS_1)^P_{\min}$ and $(ZS_1)^M_{\min}$] were found for Z-dMe-OMe-NAIP (Fig. 6; Tables S3 and S4, in SD). Possibly due to the decrease in steric hindrance from the removal of the methyl group at C5, Z-dMe-OMe-NAIP is more planar than Z-OMe-NAIP. Consequently, $(ZS_0)^M_{\min}$ is characterized by less twisting around the C1'-C4 double bond ($\tau_a = -168^\circ$) and the S_1 vertical energy is 2.94 eV, close to that of the E configuration (3.00 eV).

Similar to OMe-NAIP, four types of S_1/S_0 CI minima are found for dMe-OMe-NAIP at the OM2/MRCI level (Fig. 6; Tables S3 and S4, in SD). The first and second S_1/S_0 conical intersection $(CI)_\alpha^M$ (1.95 eV)

and $(CI)_\beta^M$ (1.96 eV) are characterized by different twisting motions around the C1'-C4 double bond, namely $\tau_a = -72^\circ$ and $\tau_a = -108^\circ$, respectively. For both of them, strong pyramidalization of the C1' atom ($\tau_b = \pm 21^\circ$) and elongation of the C1'-C4 bond ($r_a = 1.45 \text{ \AA}$) were observed. Similarly, the third and fourth CI minima can also be found, though they have only minor contributions to the nonadiabatic dynamics of dMe-OMe-NAIP and thus are not discussed here.

Because dMe-OMe-NAIP is not widely studied theoretically, we also performed high-level CASSCF/CASPT2 and SCS-ADC(2) calculations to check the validity of the OM2/MRCI method. Single-point calculations were performed at all critical geometries obtained at the OM2/MRCI level and the relevant energies at the ground and excited state minima are consistent. At the first two CI geometries obtained at the OM2/MRCI level, CASPT2 shows that the S_0-S_1 energy gap is small. Although they are not exactly degenerate,

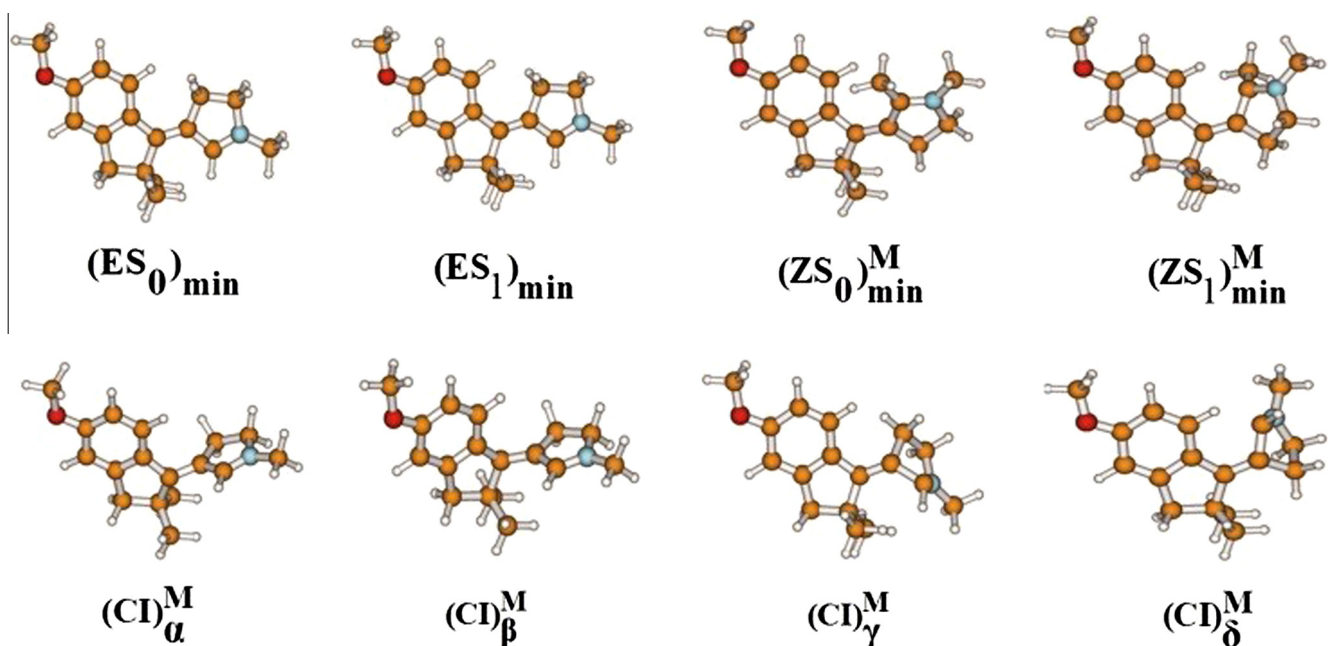


Fig. 6. The S_0 , S_1 minima and CIs of the M conformer of dMe-OMe-NAIP optimized at the OM2/MRCI level.

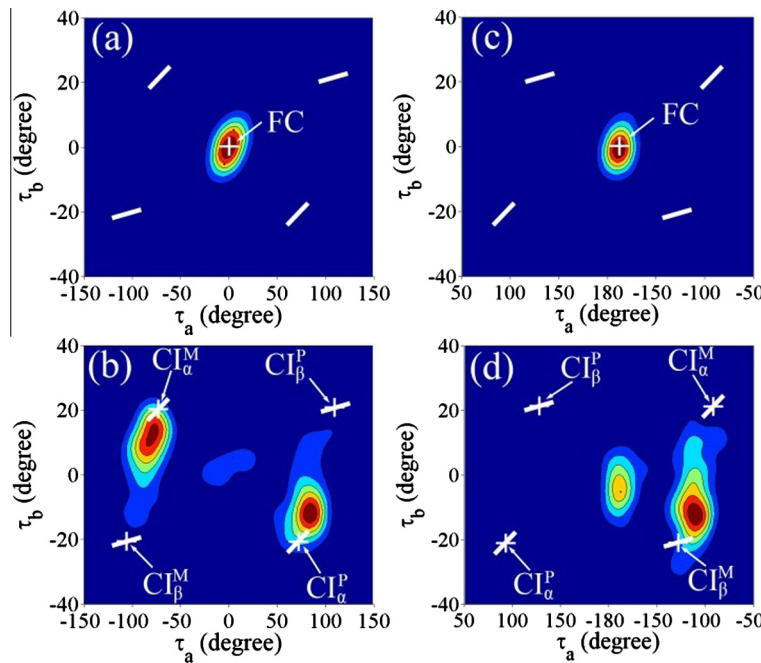


Fig. 7. Geometrical distributions of τ_a and τ_b at: (a) initial steps for E-dMe-OMe-NAIP; (b) hopping steps for E-dMe-OMe-NAIP; (c) initial steps for Z-dMe-OMe-NAIP; (d) hopping steps for Z-dMe-OMe-NAIP. The white lines indicate the CI seams. Note that the x axes (τ_a) in the above figures ($[-150, 150]$ in the left column and $[50, -50]$ in the right column) are not displayed in the same region.

these data indicate the reasonability of the CI geometries obtained at the OM2/MRCI level. In addition, OM2/MRCI and CASPT2 gave the similar main reaction pathways (Figs. S21 and S22, in SD). All of these details are found in SD.

3.2.2. Nonadiabatic dynamics of dMe-OMe-NAIP

For E-dMe-OMe-NAIP, the single S_0 minimum $(ES_0)_{\min}$ as chosen as the reference geometry for initial sampling. For Z-dMe-OMe-NAIP, we chose $(ZS_0)_{\min}^M$ is the starting point in the initial sampling.

After photo-excitation to S_1 , both isomers, E-dMe-OMe-NAIP and Z-dMe-OMe-NAIP, display ultrafast $S_1 \rightarrow S_0$ decay (Fig. 2(c) and (d)). More than 50% of the trajectories jump to the S_0 state after approximately 1000 fs. Although such decays are also ultrafast, they take place at much longer time-scales than the same nonadiabatic processes for OMe-NAIP. Although our simulation cannot accurately reproduce the lifetime of dMe-OMe-NAIP from the experimental observation, this work clearly demonstrates that the removal of the methyl group in fact causes the slower decay in the photoinduced E/Z isomerization.

For E-dMe-OMe-NAIP (Fig. 7(a) and (b)), the center of the initial distribution is located at the FC point ($\tau_a = 0^\circ$, $\tau_b = 0^\circ$) because $(ES_0)_{\min}$ is planar. The majority of trajectories passed CI seams near $(Cl)_\alpha$ and $(Cl)_\beta$ by the twisting motion around the C1'-C4 double bond and the pyramidalization at C1', whereas $(Cl)_\alpha$ is highly preferred over $(Cl)_\beta$. The elongation of the C1'-C4 bond is observed along the trajectory propagation from the FC region to the relevant CIs (see SD). Similar nuclear motions are observed for E-OMe-NAIP as well, and the possible underlying reasons are discussed previously in Section 3.1.2. Because the initial geometry is planar, both $(Cl)_\alpha$ isomers [$(Cl)_\alpha^P$ and $(Cl)_\alpha^M$] play equivalent roles and the chirality selectivity vanishes. A minority of the trajectories passed CI seams near $(Cl)_\gamma$ by the pyramidalization at C2.

For Z-dMe-OMe-NAIP (Fig. 7(c) and (d)), the dynamics go back to the normal helicity selectivity and most hops take place around $\tau_a = -108^\circ$ for the M configuration because the S_0 minimum is not

planar. The primary reaction channel passed $(Cl)_\beta^M$ because it is closer to the FC point.

As with OMe-NAIP, the $(Cl)_\alpha$ and $(Cl)_\beta$ seams are responsible for the decay of E-dMe-OMe-NAIP and Z-dMe-OMe-NAIP, respectively (Fig. 5(c) and (d)). Although some other channels seem to become involved, we neglect them and focus on the major channels here because we wish to emphasize the primary differences between OMe-NAIP and dMe-OMe-NAIP.

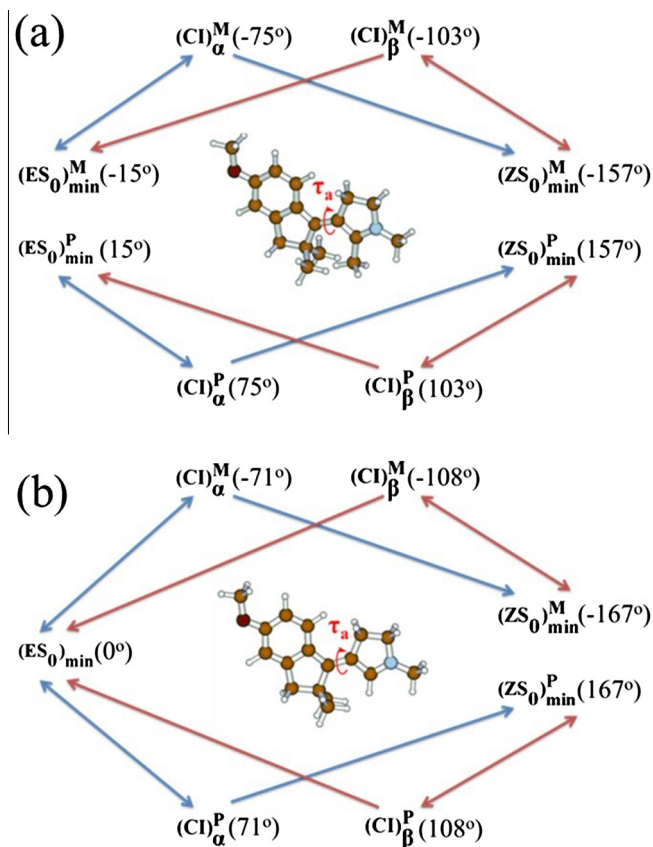
4. Discussion

Two NAIP-based switches (OMe-NAIP and dMe-OMe-NAIP) were studied by the surface-hopping method. Both have two stable configurations (E and Z) which can be interconverted via photoinduced isomerization. The overall mechanism of the E \rightarrow Z and Z \rightarrow E isomerizations of OMe-NAIP (Scheme 3(a)) and dMe-OMe-NAIP (Scheme 3(b)) are constructed.

For all configurations (E-OMe-NAIP, Z-OMe-NAIP, E-dMe-OMe-NAIP and Z-dMe-OMe-NAIP), the S_0 and S_1 minima structures were found at the OM2/MRCI level. Most of these minima structures have two conformers (P and M) which are symmetrical with each other. The only exception is the $(ES_0)_{\min}$ of dMe-OMe-NAIP, which has only one conformer with a planar structure.

The removal of the methyl group from OMe-NAIP eliminates the steric hindrance in dMe-OMe-NAIP and thus the ground-state equilibrium geometry should display less distortion. For example, the absolute value of the central C1'-C4 twisting angle τ_a changes from 157° (Z-OMe-NAIP) to 167° (Z-dMe-OMe-NAIP). For the E isomers, such effects become even more significant because $(ES_0)_{\min}$ shows no twist at the C1'-C4 bond in dMe-OMe-NAIP.

For OMe-NAIP and dMe-OMe-NAIP, four types of CIs [$(Cl)_\alpha$, $(Cl)_\beta$, $(Cl)_\gamma$ and $(Cl)_\delta$] are found, although only $(Cl)_\alpha$ and $(Cl)_\beta$ play essential roles in the nonadiabatic decay. To explain this, potential energy profiles were constructed from the S_0 minima to the relevant CIs for OMe-NAIP (Figs. S11 and S12, in SD) and



Scheme 3. The mechanism of E → Z and Z → E isomerization for (a) OMe-NAIP and (b) dMe-OMe-NAIP. The arrows indicate the main reaction channels. The dihedral angle τ_a is given for each geometry.

dMe-OMe-NAIP (Figs. S13 and S14, in SD). It is clear that $(Cl)_\alpha$ and $(Cl)_\beta$ instead of $(Cl)_\gamma$ and $(Cl)_\delta$ are mainly responsible for the nonadiabatic decay of these two systems. Additionally, in our benchmark calculations, the S_0 and S_1 PESs along the excited-state reaction pathway at high levels [CASPT2 and SCS-ADC(2)] were also constructed by the linear interpolation from the S_0 minima to main CIs [$(Cl)_\alpha^M$ and $(Cl)_\beta^M$] (Figs. S19–S22, in SD). The PES profiles were comparable with those at OM2/MRCI level. This confirms that the semi-empirical OM2/MRCI method provides a reasonable description of the photodynamical processes of current molecules.

The overall dynamics are shown in Scheme 3. Interestingly, regardless of the inclusion of the CH_3 group, the E → Z reactions always prefer $(Cl)_\alpha$, whereas $(Cl)_\beta$ becomes dominant for the reversed Z → E isomerization. In other words, the forward and backward isomerization dynamics primarily follow different reaction channels. The reason seems to be obvious: $(Cl)_\alpha$ is close to the E configuration and $(Cl)_\beta$ is close to the Z configuration. Thus, trajectories starting from the E configuration should pass $(Cl)_\alpha$ before $(Cl)_\beta$ and the reverse situation is true for trajectories from the Z configuration. We also found that the trajectories passing two CIs could rotate forwards to the photoproducts or return backwards to the initial reactants.

Interestingly, the sign of τ_a remained unchanged during the nonadiabatic dynamics. It is apparent that the **P** and **M** chirality feature (with respect to the rotation along the C1'–C4 bond) is maintained during E → Z and Z → E isomerizations. Strong steric hindrance may appear if the system accesses geometries with $\tau_a \sim 0^\circ$ or 180° . Note that the dynamics from $(ES_0)_{min}$ are special

because the initial geometry is planar and thus both **P** and **M** isomers are accessed.

One major difference between the nonadiabatic dynamics of OMe-NAIP and dMe-OMe-NAIP is their lifetime. This may also be attributed to different initial geometries. As discussed above, the system becomes more planar from OMe-NAIP to dMe-OMe-NAIP, while their Cl geometries are similar. The system must therefore experience more rotation before accessing the Cl seams on the excited states, requiring a longer time for dMe-OMe-NAIP to reach the S_0/S_1 CI. In addition, the S_1 PES is very flat in the area with small τ_a , making it more difficult for dMe-OMe-NAIP to escape that region on the S_1 PES. As a result, the decay of dMe-OMe-NAIP becomes much slower.

Although our calculated lifetime of dMe-OMe-NAIP is longer than the experimental data (~ 500 fs) [47], we still believe that the overall simulation results provide some useful conclusions, at least in a qualitative manner. First, the energies at all critical geometries and PESs along the reaction pathways of OMe-NAIP and dMe-OMe-NAIP at the OM2/MRCI level are basically consistent with high-level calculations in previous work [44] and in the current study (Tables S1–S4, Figs. S19–S22, in SD). This indicates that the PESs of these two systems are reasonable at the OM2/MRCI level, thus the dynamics results at OM2/MRCI level are trustable. Second, the simulation of OMe-NAIP provides ultrafast nonadiabatic dynamics within 300 fs, highly consistent with previous experimental studies and theoretical work [44]. Third, the slowdown of the excited-state decay by removing the CH_3 group is clearly identified by the current dynamics simulations. Concerning the reasonable performance of OM2/MRCI in ordinary organic systems [51–63,86–88], we believe that the present calculation effectively captures the main features of the E/Z isomerization of dMe-OMe-NAIP and OMe-NAIP.

As discussed in Figs. S19 and S20 in SD, we should not neglect the deviation (<0.2 eV) of the reaction pathway at the OM2/MRCI level and more accurate CASPT2 level. Such deviation may bring different features in the excited state dynamics. It is true that the discrepancy in the decay timescales between the experimental and theoretical works should not be fully neglected, and such differences may come from the substantial errors of the semi-empirical OM2/MRCI method or the lack of solvent environments. In addition, when the starting geometry is planar, the PESs become very flat in the FC region. A slight deviation in initial conditions or PESs may result in very different time durations for the system escaping that region. To clarify these problems, the nonadiabatic dynamics of dMe-OMe-NAIP and OMe-NAIP should be re-examined by surface-hopping dynamics with high-level theories (even with QM/MM approaches), which in principle should involve a large number of trajectories for statistical reasons. However, due to large computational costs, such calculations are very difficult, and it is thus still reasonable to employ the OM2/MRCI method to understand the E/Z isomerization dynamics of NAIP and its derivatives. In particular, because of the large number of trajectories considered in this work, the trajectory surface-hopping calculation provides the primary understanding of the nonadiabatic dynamics of NAIP-based molecular switches, at least in qualitative or semi-quantitative respects. In this sense, the current work also serves as an important foundation for future dynamics simulations with high-level electronic-structure theories.

5. Conclusions

In this work, the photoinduced E → Z or Z → E isomerization mechanism of two NAIP-based molecular switches, OMe-NAIP and dMe-OMe-NAIP, were investigated by on-the-fly Tully surface-hopping methods at the semi-empirical OM2/MRCI level.

The excited-state reaction pathways were characterized by critical geometries, including the relevant electronic states, energy minima and conical intersections. We focused on the ultrafast $S_1 \rightarrow S_0$ nonadiabatic dynamics responsible for the isomerization of NAIP-based compounds.

Two main channels are responsible for $E \rightarrow Z$ or $Z \rightarrow E$ isomerization for both NAIPs. The $E \rightarrow Z$ dynamics are mainly governed by $C\alpha$, characterized by the twisting motion of the C1'–C4 double bond, the pyramidalization at C1' and the elongation of the C1'–C4 bond distance. The second channel, via $C\beta$, contributes to the reversed $Z \rightarrow E$ isomerization, identified by twisting around the C1'–C4 double bond with different angles.

From OMe-NAIP to dMe-OMe-NAIP, the removal of the methyl group reduces steric hindrance, leading to a more planar molecular geometry. The distances between the FC region and Cls therefore become larger and a slower isomerization was obtained from the nonadiabatic dynamics simulations.

This finding provides more solid support to the previous joint experimental–theoretical study [47]. In other words, this work clearly demonstrated that adding or removing functional groups attached to the main skeleton may have significant influence on the isomerization features of NAIP-based photoswitches. This information can be used to design novel biomimetic molecular devices.

Conflict of interest

The authors declare no competing financial interest.

Acknowledgements

This work was supported by the CAS 100 Talents Project, National Natural Science Foundation of China (NSFC) project (Grants 21543008, 21503248, 21503156 and 91233106), Key Lab of Nanodevices and Nanoapplications, CAS (14HZ03). This work was also supported by the Natural Science Foundation of Shandong Province for Distinguished Young Scholars (JQ201103). The authors thank the Supercomputing Center, Computer Network Information Center, CAS, national supercomputing center in Shenzhen and the supercomputational center of CAS-QIBEBT for providing computational resources.

Appendix A. Supplementary data

Supplementary data associated with this article can be found, in the online version, at <http://dx.doi.org/10.1016/j.chemphys.2015.10.003>.

References

- [1] B.L. Feringa, W.R. Browne, in: *Molecular Switches*, Wiley-VCH Verlag GmbH & Co. KGaA, 2011, p. I.
- [2] A. Kazaryan, J.C.M. Kistemaker, L.V. Schafer, W.R. Browne, B.L. Feringa, M. Filatov, *J. Phys. Chem. A* **114** (2010) 5058.
- [3] Y. Shiraishi, S. Sumiya, T. Hirai, *Chem. Commun.* **47** (2011) 4953.
- [4] N. Shao, J. Jin, H. Wang, J. Zheng, R. Yang, W. Chan, Z. Abliz, *J. Am. Chem. Soc.* **132** (2009) 725.
- [5] H. Zhang, X.X. Kou, Q. Zhang, D.H. Qu, H. Tian, *Org. Biomol. Chem.* **9** (2011) 4051.
- [6] T. Muraoka, K. Kinbara, T. Aida, *J. Am. Chem. Soc.* **128** (2006) 11600.
- [7] M. McCullagh, I. Franco, M.A. Ratner, G.C. Schatz, *J. Am. Chem. Soc.* **133** (2011) 3452.
- [8] M. Singer, A. Jäschke, *J. Am. Chem. Soc.* **132** (2010) 8372.
- [9] J. Andersson, S. Li, P. Lincoln, J. Andréasson, *J. Am. Chem. Soc.* **130** (2008) 11836.
- [10] X. Su, I. Aprahamian, *Chem. Soc. Rev.* **43** (2014) 1963.
- [11] R. Klajn, *Chem. Soc. Rev.* **43** (2014) 148.
- [12] G. Vantomme, J.M. Lehn, *Angew. Chem. Int. Ed.* **52** (2013) 3940.
- [13] W.F. Yuan, L. Sun, H.H. Tang, Y.Q. Wen, G. Jiang, W. Huang, L. Jiang, Y.L. Song, H. Tian, D.B. Zhu, *Adv. Mater.* **17** (2005) 156.
- [14] G. Berkovic, V. Krongauz, V. Weiss, *Chem. Rev.* **100** (2000) 1741.
- [15] H. DürrHenri, in: H.D. Bouas-Laurent (Ed.), *Photochromism: Molecules and Systems*, Elsevier Science, Amsterdam, 1990, p. 1.
- [16] H. Dube, D. Ajami, J. Rebek, *Angew. Chem. Int. Ed.* **49** (2010) 3192.
- [17] O. Weingart, Z. Lan, A. Koslowski, W. Thiel, *J. Phys. Lett.* **2** (2011) 1506.
- [18] R. Siewertsen, J.B. Schoenborn, B. Hartke, F. Renth, F. Temps, *Phys. Chem. Chem. Phys.* **13** (2011) 1054.
- [19] J. Bao, P.M. Weber, *J. Am. Chem. Soc.* **133** (2011) 4164.
- [20] J.A. Gamez, O. Weingart, A. Koslowski, W. Thiel, *Phys. Chem. Chem. Phys.* **15** (2013) 11814.
- [21] J.A. Gamez, O. Weingart, A. Koslowski, W. Thiel, *J. Chem. Theory Comput.* **8** (2012) 2352.
- [22] A. Clossen, W.R. Browne, B.L. Feringa, *Top. Curr. Chem.* **354** (2014) 139.
- [23] G. Perez-Hernandez, L. Gonzalez, *Phys. Chem. Chem. Phys.* **12** (2010) 12279.
- [24] E.M. Geertsema, R. Hoen, A. Meetsma, B.L. Feringa, *Eur. J. Org. Chem.* **16** (2006) 3596.
- [25] M.K.J. ter Wiel, A. Meetsma, B.L. Feringa, *Tetrahedron* **58** (2002) 2183.
- [26] A.V. Struts, G.F.J. Salgado, C. Job, K. Tanaka, S. Krane, K. Nakanishi, M.F. Brown, *Biophys. J.* **88** (2005) 222A.
- [27] U.F. Rohrig, L. Guidoni, U. Rothlisberger, *Chem. Phys. Chem.* **6** (2005) 1836.
- [28] N.E. Fishkin, J.R. Sparrow, R. Allikmets, K. Nakanishi, *Proc. Natl. Acad. Sci. U.S.A.* **102** (2005) 7091.
- [29] M. Garavelli, T. Vreven, P. Celani, F. Bernardi, M.A. Robb, *J. Am. Chem. Soc.* **120** (1998) 1285.
- [30] G. Hayward, W. Carlsen, A. Siegman, L. Stryer, *Science* **211** (1981) 942.
- [31] C. García-Iriepa, M. Marazzi, L.M. Frutos, D. Sampedro, *RSC Adv.* **3** (2013) 6241.
- [32] B. Schierling, A.J. Noel, W. Wende, L.T. Hien, E. Volkov, E. Kubareva, T. Oretskaya, M. Kokkinidis, A. Rompp, B. Spengler, et al., *Proc. Natl. Acad. Sci. U.S.A.* **107** (2010) 1361.
- [33] B. Buchli, S.A. Waldauer, R. Walser, M.L. Donten, R. Pfister, N. Blochiger, S. Steiner, A. Caflisch, O. Zerbe, P. Hamm, *Proc. Natl. Acad. Sci. U.S.A.* **110** (2013) 11725.
- [34] S.L. Broman, M.B. Nielsen, *Phys. Chem. Chem. Phys.* **16** (2014) 21172.
- [35] D. Polli, P. Altoe, O. Weingart, K.M. Spillane, C. Manzoni, D. Brida, G. Tomasello, G. Orlandi, P. Kukura, R.A. Mathies, et al., *Nature* **467** (2010) 440.
- [36] I. Rivalta, A. Nenov, M. Garavelli, *Phys. Chem. Chem. Phys.* **16** (2014) 16865.
- [37] O. Weingart, M. Garavelli, *J. Chem. Phys.* **137** (2012) 22A523.
- [38] O. Weingart, *J. Am. Chem. Soc.* **129** (2007) 10618.
- [39] V. Buss, O. Weingart, M. Sugihara, *Angew. Chem. Int. Ed.* **39** (2000) 2784.
- [40] X. Li, L.W. Chung, K. Morokuma, *J. Chem. Theory Comput.* **7** (2011) 2694.
- [41] L.H. Andersen, I.B. Nielsen, M.B. Kristensen, M.O.A.E.I. Ghazaly, S. Haacke, M.B. Nielsen, M.A. Petersen, *J. Am. Chem. Soc.* **127** (2005) 12347.
- [42] G. Marchand, J. Eng, I. Schapiro, A. Valentini, L.M. Frutos, E. Pieri, M. Olivucci, J. Léonard, E. Gindensperger, *J. Phys. Chem. L.* **6** (2015) 599.
- [43] A. Melloni, R. Rossi Paccani, D. Donati, V. Zanirato, A. Sinicropi, M.L. Parisi, E. Martin, M. Ryazantsev, W.J. Ding, L.M. Frutos, et al., *J. Am. Chem. Soc.* **132** (2010) 9310.
- [44] A. Sinicropi, E. Martin, M. Ryazantsev, J. Helbing, J. Briand, D. Sharma, J. Leonard, S. Haacke, A. Cannizzo, M. Chergui, et al., *Proc. Natl. Acad. Sci. U.S.A.* **105** (2008) 17642.
- [45] F. Lumento, V. Zanirato, S. Fusi, E. Busi, L. Latterini, F. Elisei, A. Sinicropi, T. Andruniow, N. Ferre, R. Basosi, et al., *Chem. Int. Ed.* **46** (2007) 414.
- [46] L.M. Frutos, T. Andruniow, F. Santoro, N. Ferré, M. Olivucci, *Proc. Natl. Acad. Sci. U.S.A.* **104** (2007) 7764.
- [47] A.D. Dunkelberger, R.D. Kieda, J.Y. Shin, R. Rossi, *J. Phys. Chem. A* **116** (2012) 3527.
- [48] E. Fabiano, T.W. Keal, W. Thiel, *Chem. Phys.* **349** (2008) 334.
- [49] S. Hammes-Schiffer, J.C. Tully, *J. Chem. Phys.* **101** (1994) 4657.
- [50] J.C. Tully, *J. Chem. Phys.* **93** (1990) 1061.
- [51] N. Otte, M. Scholten, W. Thiel, *J. Phys. Chem. A* **111** (2007) 5751.
- [52] W. Weber, W. Thiel, *Theor. Chem. Acc.* **103** (2000) 495.
- [53] W. Weber, *Parametrizierung Und Anwendungen*, Universität Zürich, Zürich, Switzerland, 1996.
- [54] B. Heggen, Z. Lan, W. Thiel, *Phys. Chem. Chem. Phys.* **14** (2012) 8137.
- [55] X. Zhuang, J. Wang, Z. Lan, *J. Phys. Chem. B* **117** (2013) 15976.
- [56] X. Zhuang, J. Wang, Z. Lan, *J. Phys. Chem. A* **117** (2013) 4785.
- [57] Z. Lan, Y. Lu, O. Weingart, W. Thiel, *J. Phys. Chem. A* **116** (2012) 1510.
- [58] J.B. Schonborn, B. Hartke, *Phys. Chem. Chem. Phys.* **16** (2014) 2483.
- [59] J.B. Schonborn, A. Koslowski, W. Thiel, B. Hartke, *Phys. Chem. Chem. Phys.* **14** (2012) 12193.
- [60] J.A. Gamez, A. Koslowski, W. Thiel, *RSC Adv.* **4** (2014) 1886.
- [61] A. Kazaryan, Z. Lan, L.V. Schäfer, W. Thiel, M. Filatov, *J. Chem. Theory Comput.* **7** (2011) 2189.
- [62] L. Sporkel, G.L. Cui, W. Thiel, *J. Phys. Chem. A* **117** (2013) 4574.
- [63] G.L. Cui, Z.G. Lan, W. Thiel, *J. Am. Chem. Soc.* **134** (2012) 1662.
- [64] A.D. McNaught, *Compendium of Chemical Terminology*, vol. 1669, Blackwell Science Oxford, 1997.
- [65] W.J.A. Woittiez, *Advanced organic chemistry, Reactions, Mechanisms, and Structure*, fourth ed., Recl. Trav. Chim. Pays-Bas, 1993.
- [66] F. Liu, K. Morokuma, *J. Am. Chem. Soc.* **134** (2012) 4864.
- [67] W. Thiel, MnDO Program, Version 7.0: Max-Planck-Institut für Kohlenforschung: Mülheim an der Ruhr, Germany, 2005.
- [68] V.N. Glushkov, *Opt. Spectrosc.* **91** (2001) 196.
- [69] T.W. Keal, A. Koslowski, W. Thiel, *Theor. Chem. Acc.* **118** (2007) 837.
- [70] D.R. Yarkony, *Rev. Mod. Phys.* **68** (1996) 985.

- [71] K. Andersson, P.A. Malmqvist, B.O. Roos, A.J. Sadlej, K. Wolinski, *J. Phys. Chem.* 94 (1990) 5483.
- [72] S. Grimme, *J. Chem. Phys.* 118 (2003) 9095.
- [73] A. Hellweg, S.A. Grun, C. Hattig, *Phys. Chem. Chem. Phys.* 10 (2008) 4119.
- [74] J. Auerswald, B. Engels, I. Fischer, T. Gerbich, J. Herterich, A. Krueger, M. Lang, H.C. Schmitt, C. Schon, C. Walter, *Phys. Chem. Chem. Phys.* 15 (2013) 8151.
- [75] J. Schirmer, *Phys. Rev. A* 26 (1982) 2395.
- [76] F. Aquilante, T. Todorova, T.B. Pedersen, L. Gagliardi, B.O. Roos, *J. Chem. Phys.* 131 (2009) 034113.
- [77] F. Aquilante, L. De Vico, N. Ferré, G. Ghigo, *J. Comput. Chem.* 31 (2010) 224.
- [78] R. Ahlrichs, M. Bar, M. Haser, H. Horn, C. Kolmel, *Chem. Phys. Lett.* 162 (1989) 165.
- [79] E. Wigner, *Phys. Rev.* 40 (1932) 749.
- [80] G. Granucci, M. Persico, *J. Chem. Phys.* 126 (2007) 134114.
- [81] L. Salem, *Acc. Chem. Res.* 12 (1979) 87.
- [82] M. Ben-Nun, *Chem. Phys.* 259 (2000) 237.
- [83] J.-Y. Fang, S. Hammes-Schiffer, *J. Phys. Chem. A* 103 (1999) 9399.
- [84] N. Shenvi, J.E. Subotnik, W. Yang, *J. Chem. Phys.* 134 (2011) 144102.
- [85] C. Zhu, S. Nangia, A.W. Jasper, D.G. Truhlar, *J. Chem. Phys.* 121 (2004) 7658.
- [86] L. Spörkel, G. Cui, W. Thiel, *J. Phys. Chem. A* 117 (2013) 4574.
- [87] B. Xie, S. Xia, L. Liu, G. Cui, *J. Phys. Chem. A* 119 (2015) 5607.
- [88] S. Xia, B. Xie, Q. Fang, G. Cui, W. Thiel, *Phys. Chem. Chem. Phys.* 17 (2015) 9687.